Workshop on Virtual Reality Interaction and Physical Simulation VRIPHYS (2014)
J. Bender, C. Duriez, F. Jaillet, and G. Zachmann (Editors)

Information Fusion for Real-time Motion Estimation in Image-guided Breast Biopsy Navigation

Bojan Kocev[1,2], Joachim Georgii[1], Lars Linsen[2], Horst Karl Hahn[1,2]

[1]Fraunhofer MEVIS, Bremen, Germany
[2]Jacobs University, Bremen, Germany

Abstract

A real-time delivery of accurate soft-tissue intervention navigation information is one of the most crucial aspects for accepting the soft-tissue navigation systems for intra-operative use. Currently, soft-tissue navigation systems face some obstacles in terms of registration of the virtual navigation information on the deformable soft-tissue organ. Most of them perform a rigid registration between the virtual data and the organ, and then provide the surgeon with all navigation information. However, they suffer from the disadvantage that the virtual information is not correctly registered to the deformable organ. In order to enable a real-time non-linear registration between the virtual navigation information and the deformable organ, we incorporate different means for tracking the soft-tissue internal and on-surface local motion. Furthermore, we introduce an intelligent information fusion engine for combining the various soft-tissue local motion tracking information into a global motion information channel. The fusion engine is the interface to the motion measurements, a motion dynamics model, and static shape information, which are combined to compute the a posteriori estimate of the current state of the deformed shape. The dynamics model is realized as a finite-element deformation simulation. In order to test the feasibility of our devised information fusion engine, we have employed it for capturing the global motion of a breast phantom during an image-guided biopsy. The biopsy planning navigation data, in the form of a prior diagnostic MRI, is continuously updated over time according to the a posteriori estimate of the global motion. As a result, the real-time changes in the shape of the breast are always reflected in the biopsy navigation information.

Categories and Subject Descriptors (according to ACM CCS): I.4.8 [Image Processing and Computer Vision]: Scene Analysis—Motion, Sensor fusion, Tracking, Shape; J.3 [Computer Applications]: Life and Medical Sciences—Health

1. Introduction

Smart information processing and interactive visualization systems have advanced significantly over the past years, while fascinating us in many different ways. One of the most prominent fields in which the incorporation of such systems is very beneficial, is the field of modern medical technology for computer-assisted intervention planning and navigation. Currently, modern medical technologies employing such systems are widely accepted for pre-operative planning and diagnosis. However, their intra-operative use is still facing some obstacles in terms of intervention navigation and surgeon's interaction with the virtual information system. The problem in terms of intervention navigation is twofold:

1. there are *inaccuracies in the registration* of the navigation information on the deformable soft-tissue organ [MMHW*08], and
2. there is *an increase in the cognitive load* of the intervention specialist during the transfer of the navigation information from the system to the intervention situs.

The inaccuracies in the registration of the navigation information on the deformable soft-tissue organ are, in general, due to the rigid registration between the virtual data and the soft-tissue organ or due to incomplete and erroneous soft-tissue motion tracking. In other words, the deformation component of the motion, which the soft-tissue organ undergoes over time, is not properly taken into account.
The obstacles in terms of surgeon's interaction with the virtual information are related to the fact that the *navigation system is usually placed far away* from the surgeon which

DOI: 10.2312/vriphys.20141227

inhibits direct interaction.
Projector-based soft-tissue navigation and surgeon-computer natural interaction mechanisms [KOP11, KRL13] are very promising in circumventing the obstacles concerning the transfer of the virtual navigation information and the difficulties in the interaction therewith. *However, the overall acceptance of the navigation systems as beneficial for the intra-operative medical interventions is still confronting big challenges, mainly due to the inaccuracies in the registration of the navigation information on the deformable soft-tissue organ.*

1.1. Information Fusion System

In order to increase the accuracy of the above-described registration task, we devised an intelligent information fusion engine for real-time estimation of the motion that a tracked instance undergoes over time. The engine fuses, in real time, three information sources: motion dynamics, motion measurements, and shape information of the tracked instance whose motion is being estimated.

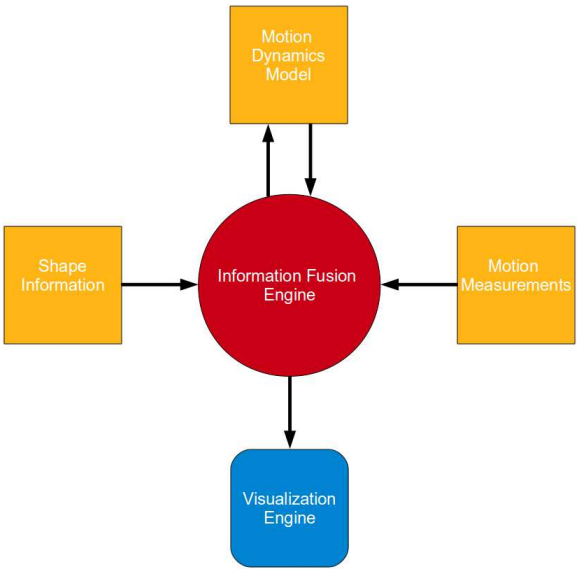

Figure 1: *General Information Fusion Concept.*

The tracked instance is represented in a discrete fashion (see Section 3), and its motion state at any discrete time k is directly defined by the positions of all points which constitute its discrete representation. The information fusion is performed at the points which constitute the discrete representation of the tracked instance. In accordance with this, the information sources are estimated on a per-point basis, at the points which constitute the state of the tracked instance. Our navigation information visualization engine is then able to update the virtual navigation information, in real time, according to the output of our intelligent information fusion engine, such that the changes in the pose and shape of the tracked instance are reflected in the displayed virtual information. The general concept for the above-described information fusion, with an accompanying navigation information visualization engine, is depicted in Figure 1. In this regard, the work of Comaniciu et al. [CZK04] was influential to us in our formulation of the general information fusion problem in this manner.
In this work, we actually present the solution of a specific information fusion problem instance, depicted in Figure 2.

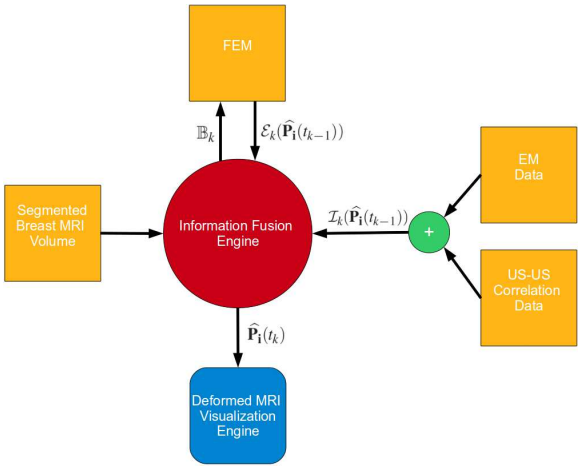

Figure 2: *Information fusion problem instance in the context of breast biopsy navigation. $\mathcal{E}_k$ is the a priori displacement estimate (taking into account the set of boundary conditions $\mathbb{B}_k$) and $\mathcal{I}_k$ is the approximation of the measurement displacement vectors information source at a specific state point, at a discrete time index k. $\widehat{\mathbf{P}}_\mathbf{i}(t_k)$ is the a posteriori estimate of the position of state point $\mathbf{P}_\mathbf{i}$, at time t_k.*

The motion dynamics modeling is embedded in a finite element model (see Section 5), which is set with parameters specific to the instance whose motion is being estimated. The finite element model is then used to simulate in real time the motion dynamics of the tracked instance, which serves as a prediction of the motion which the tracked instance undergoes over a specified time period. Furthermore, the finite element-based model is actually extracted from a segmented volumetric scan of the instance whose motion is being estimated. In other words, the shape information is also embedded into the finite element-based model. Therefore, the prediction $\mathcal{E}_k$ (see Figure 2) by our finite element-based nonlinear motion prediction model is actually the fusion of the motion system dynamics and the shape information sources. The motion measurements information source is composed of real-time surface (electromagnetic-based) and volumetric (ultrasound-based) tracking data (see Section 4), which captures the motion of the tracked instance at points which do not necessarily correspond in number as well as physically to the points constituting the state of the tracked in-

stance. Therefore, the displacement vectors, which describe the change in the position of all tracked points from time $k-1$ to k, are interpolated at the discrete points which constitute the state of the tracked instance. In that way, we obtain the approximation $\mathcal{I}_k$ (see Figure 2) of the measurement displacement vectors information source at the state points.
The overall information fusion and estimation of the a posteriori state $\widehat{\mathbf{P}}$ (see Figure 2) are described in Section 6. The virtual navigation information, in the form of a prior diagnostic MRI, is updated in real time according to the output of our intelligent information fusion engine (see Section 7), such that it always reflects the estimated current shape and internal structure of the tracked instance. Since the overall information fusion and navigation information update is performed in real time, we need to exploit concurrency and parallelism efficiently and correctly (see Section 8). Results are presented and discussed in Section 9.

1.2. Contribution

Our main contribution to the state of the art can be summarized as follows:

1. real-time information fusion engine for motion measurements, motion dynamics, and shape information to estimate the a posteriori motion state and visualize the deformed shape;
2. computation and integration of displacements from measurements and models;
3. application to real-time image-guided breast-biopsy navigation.

2. Related Work

Baumhauer et al. [BFMR08] pointed out that probably the greatest challenge, in the field of computer assisted navigation for endoscopic soft tissue interventions, relates to the intraoperative measurement and modeling of organ shift and tissue deformation of "unconstrained" organs in thoracic and abdominal cavities. Furthermore, they noted that as navigation is performed over certain period of time, a continuous correction of tissue motion and deformation would be required for constant and reliable navigation accuracy. In this section, we will discuss a list of selected related work of others about: measurement of the organ shift and tissue deformations, soft tissue deformation modeling, and information fusion of these and related information sources.
Zhang et al. [ZBL*06] employed magnetically tracked needles and biomechanical models, while compensating the liver respiratory motion. They have implemented and extended the so-called paired-point, sensor orientation-based, and needle-based (needles are implanted in the soft-tissue organ and sampled both in the electromagnetic space as well as in the CT image space) registration methods. Furthermore, they rely on the affine transform proposed by Horn [Hor87] for simulating the small-range deformation.
Kocev et al. [KRL13] incorporated an algorithm for creating, in real time, a virtual point-based representation of the deformable surface of a tracked instance lying on a surgical table. They first create a virtual point-based model of the whole scene (viewed by a Kinect camera), and then segment the surface of the tracked instance in the acquired point cloud. In this way, they are able to sample the global motion signal of the deformable tracked instance over time on the surface spatial domain. However, they do not sample on the tracked instance's interior spatial domain and their method may suffer from occlusion problems whenever parts of the tracked region are not seen by the Kinect camera.
Cash et al. [CMS*05] employed a range scan point cloud acquired from the exposed soft-tissue organ surface, which is then rigidly aligned to a preoperative (predeformed) complete three-dimensional surface of the organ. They account for the deformation by using a linearly elastic FEM, which is implemented by using an incremental framework to resolve geometric nonlinearities. The boundary conditions for the incremental formulation are generated from the intraoperatively acquired range scan surfaces of the exposed soft-tissue organ surface. However, they do not measure the organ interior local deformation, but rely solely on the FEM constrained with the surface boundary conditions.
Several research groups have developed methods for brain shift compensation. Škrinjar et al. [ŠND02] proposed a biomechanical-model-based approach for brain shift comensation, which is guided by limited intraoperative (exposed brain) surface data. Dumpuri et al. [DTD*07, DTC*10] computed an atlas of model deformations based on different loading conditions preoperatively, and used it with a constrained linear inverse model to predict the intra- and post-operative distributed brain shift. Miller et al. [MHJW12] employed the so-called Meshless Total Lagrangian Explicit Dynamics Method (MTLED), for computing brain deformations during surgery. The problem geometry is based on patient-specific MRI data, while the nodes are distributed automatically through the domain. They reported a Hausdorff distance difference between previously validated Finite Element results and their meshless results of less than 0.2 mm. However, in the context of real-time breast motion estimation, handling the motion deformation component might be more challenging and result in higher Hausdorff distance differences.
A relatively recent overview over ongoing research in the field of physically based deformation modeling is given by Nealen et al. [NMK*05]. For an overview over ongoing research in the field of breast biomechanics modeling, in the context of information fusion from different imaging modalities, we refer to the article by Rajagopal et al. [RNN10].
The Kalman filter, in its information filter form [AM79], is the simplest and most well-known example of fusion. It performs the fusion of the measurements and the system dynamics information sources. The measurements and the system dynamics predictions have independent uncertainty

distributions which are expressed with mean vectors and covariance matrices. Most of the other information fusion algorithms employ the original idea of Kalman for fusing the two above-mentioned information sources. However, it is often necessary to adapt or extend the Kalman fusion framework to handle additional information sources, such that more complicated motions can be estimated in an optimal and rigorous fashion.

Zhou et al. [ZGC05] continued the work of Comaniciu [CZK04], and thoroughly presented their complete information fusion framework for robust shape tracking, in a rigorous fashion. They follow the basic idea in treating the measurement, the shape model, and the prediction as noisy measurements with covariance matrices and fuse all the information in an optimal way. More specifically, they apply the subspace fusion on the Kalman fusion (measurement + prediction based on system dynamics) result and a subspace source (shape model), and in this way they combine all the available knowledge in the information space. They employ a *strongly adapted-PCA (SA-PCA)* model [CZK04] to augment the statistical generic shape model with information specific to the currently tracked shape (e.g., the initial contour of the tracked heart of a specific patient), and in this way obtain a *deformation model of the current case*. The *SA-PCA* model is then actually fused with the above-specified Kalman fusion result, such that in the end they actually fuse four information sources: the system dynamics, measurement, subspace model, and the tracked instance-specific information. In our solution, we can interpret the *finite element-based model*, extracted from the segmented volumetric scan of tracked instance, as the above-described *deformation model of the current case*. By setting the finite element-based model with tracked instance-specific material properties (density and elastic modulus), we actually incorporate the system dynamics in the finite element-based model. Therefore, the prediction of our finite element-based nonlinear motion prediction model is actually the fusion of the system dynamics and the *deformation model of the current case*.

3. Tracked Instance I^n State Representation

The tracked instance which undergoes some form of motion is denoted as I^n, where n is the number of points which constitute its discrete representation. The overall state of the tracked instance I^n, at time t, is represented by the state vector function:

$$\mathbf{S}(t) = \begin{bmatrix} \mathbf{P}_0(t) & \mathbf{P}_1(t) & \dots & \mathbf{P}_{n-1}(t) \end{bmatrix} \tag{1}$$

where $\mathbf{P}_i(t)$ is a vector variable function defined as

$$\mathbf{P}_i(t) = \begin{bmatrix} x_i(t) \\ y_i(t) \\ z_i(t) \end{bmatrix},$$

where $x_i(t)$, $y_i(t)$, and $z_i(t)$ are three scalar variables which define the 3D position, in a Cartesian coordinate system in Euclidean space, of the *i-th* point at time t. The n points P_i constitute the discrete representation of the tracked instance I^n, as shown in Figure 3.

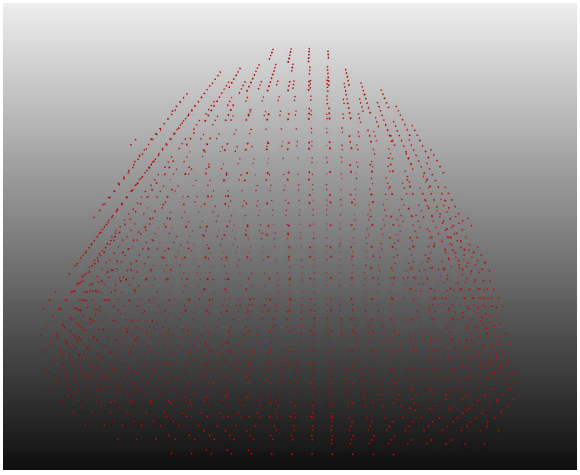

Figure 3: *Discrete representation of the breast phantom.*

The global motion of the tracked instance, from any discrete time point $k-1$ to k, is described by the displacement function:

$$u : \Omega \rightarrow \mathbb{R}^3 \tag{2}$$

where $\Omega \subset \mathbb{R}^3$ spans the 3D subspace of all possible 3D position values for the points which constitute the state representation (1) of the tracked instance I^n.

4. Motion Measurements Information Source

In general, all tracking data captures some form of motion. The measured tracking data at a discrete time point k, for an instance I^n which undergoes some form of motion, is a discrete set of points:

$$\mathbb{M}_k = \left\{ \mathbf{M_i}(t_k) : \begin{matrix} \mathbf{M_i}(t_k) \textit{ is the measurement of} \\ \textit{the } i-th \textit{ point at time } t_k \end{matrix} \right\} \tag{3}$$

whose cardinality theoretically may range from 1 to an arbitrarily large number. $\mathbf{M_i}(t_k)$ is a vector variable measurement function which gives the vector value of the observable or tracked i-th point at time t_k. In practical examples, the arbitrarily large number is sufficiently big, while the expected minimum cardinality of the set $\mathbb{M}_k$ is imposed by the minimum amount of information necessary for updating the overall state $\mathbf{S}(t_k)$ of the tracked instance correctly.

If $|\mathbb{M}_k| = n$ and $\forall \mathbf{M} \in \mathbb{M}_\mathbf{k}$ $\exists \mathbf{P_i}$ such that in reality they both correspond to the same physical point, then the state $\mathbf{S}(t_k)$ of the tracked instance I^n, at time t_k, is completely defined

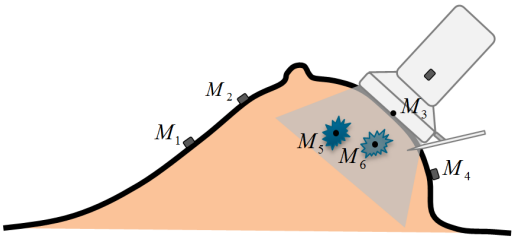

Figure 4: *Breast skin surface and interior tracking data. In this example, the discrete set of points* $\{\mathbf{M_1}, \mathbf{M_2}, \mathbf{M_3}, \mathbf{M_4}, \mathbf{M_5}, \mathbf{M_6}\}$ *constitute the set* $\mathbb{M}_k$ *from Eq. 3. The four dark gray rectangular bodies, among which three are attached directly on the skin surface and one on the utlrasound probe, are the tracked electromagnetic bodies/sensors.*

directly by the measurements. However, in real scenarios we have $|\mathbb{M}_k| < n$. Furthermore, the cardinality of the set $\mathbb{M}_k$, in general, varies and not always the same physical points are tracked over time, such that the overall spatial sampling density and coverage of the global motion signal varies from one time point to another.

Furthermore, the sets of measurements $\mathbb{M}_k$ and $\mathbb{M}_{k-1}$ define the set of samples, denoted by $\mathbb{S}_k$, from the output of the function (2) at any discrete time point k. The spatial domain Ω (defined in Eq. (2)) of the displacement function which captures the motion of the breast (treated as an I^n instance), is then the 3D subspace encompassing the breast interior and bounded by the breast skin surface. Therefore, the location of each sample $s \in \mathbb{S}_k$ could be either somewhere on the breast skin surface or in the breast interior.

In order to sample the output of the displacement function on the breast surface spatial domain, we attached small electromagnetic bodies/sensors to the breast skin surface, as illustrated in Figure 4. The 3D position of each attached electromagnetic body/sensor defines the location of a different sample from the output of the above-described displacement function, on the breast skin surface spatial domain. Furthermore, the sample values at these locations, at a discrete time k, are based on the electromagnetic tracking data, for the corresponding bodies/sensors, at the discrete time points $k-1$ and k.

In order to sample the output of the displacement function on the breast interior spatial domain, we incorporated a real-time ultrasound imaging device which is localized in the electromagnetic tracking space. This is achieved by attaching an electromagnetic body/sensor on the ultrasound probe, as illustrated in Figure 4, which enables us to localize the probe in the electromagnetic tracking space. Furthermore, we compute the position (at a discrete time k) of the contact point between the ultrasound probe and the breast skin surface, based on the tracking data (at a discrete time k) for the sensor attached on the probe and on a prior calibration of the displacement vector from the sensor location to the bottom mid point on the ultrasound probe. Moreover, we are able to use the position of this contact point as an additional sample location on the breast skin surface. Having this in hand and using a prior information about the definition of the ultrasound image space with respect to a 3D local frame positioned at the above-described contact point, we obtain the transformation between the ultrasound image space and the electromagnetic tracking space. The real-time ultrasound imaging device then captures the interior of the breast by acquiring 2D images over time, as illustrated in Figure 4. The 2D ultrasound images reveal distinctive breast soft-tissue structures, which are identified and tracked over time by a digital image correlation (DIC) variant of the real-time capable algorithms by Isard et al. [IB98] and Zhang et al. [ZGB10]. The position of every tracked point in the ultrasound image space, within the identified and tracked breast soft-tissue structures, is localized in the electromagnetic tracking 3D space, as described above. The 3D position of every tracked point, localized in the electromagnetic tracking space, then defines the location of a different sample from the output of the above-described displacement function on the breast interior spatial domain. The sample values at these locations, at a discrete time k, are then based on the DIC tracking data, for the corresponding tracked soft-tissue points, at the discrete time points $k-1$ and k.

5. Motion Dynamics and Shape Information Sources

The motion, which the tracked instance I^n undergoes between two discrete time points $k-1$ and k, in general, contains two components: a rigid-body displacement and a deformation. The rigid-body displacement is composed of a rotation and a translation component and it preserves the shape and size of the tracked instance I^n, where the change in shape and size is measured against the initial or undeformed state $\mathbf{S}(t_0)$. On the other hand, the change in the deformation component of the motion is responsible for any change in shape and size which the tracked instance I^n undergoes between the two discrete time points. The deformation component of the motion at time k has changed with respect to the one at time *k-1*, if there is a nonzero relative displacement between all or some of the points which constitute the discrete representation of the tracked instance I^n.

In our case, we need to model the dynamics of the motion which the breast undergoes over time. Soft-tissue deformation modeling is a challenging task, because it involves a major deformation component which is difficult to model when the material properties of the tracked instance I^n are not well known. Furthermore, we need an appropriate nonlinear motion model, which shall be able to predict, in real time, the change in the motion deformation component

from time *k-1* to *k*. This kind of nonlinear models in addition impose the challenge of extracting appropriate motion heuristics from the global motion signal sampling data $\mathbb{S}_k$, which are then used as boundary conditions by the nonlinear motion fitting model. In other words, the nonlinear model depends both on the time t_k and on a number of carefully selected boundary conditions to which the model is fitted, when predicting the motion deformation component.

In order to achieve a realistic soft-tissue deformation modeling, one needs to employ a physical model of the tracked instance I^n. As pointed by Georgii and Dick [GD12], physics-based modeling is preferred over simplified models, because in a physics-based prediction model the accuracy is much higher, at least, from a theoretical point of view, which is especially important for our target medical applications. Furthermore, finite elements are a well-known mathematical tool for accurate modeling of the behavior of deformable objects based on the theory of elasticity. When compared to finite difference methods, which consider only the values at discrete samples, the finite element methods take the continuum within an element into account by providing a well defined interpolation function. In this manner, a higher accuracy is guaranteed. The degree of freedom of an element is defined by the number of "free" vertices which constitute the element, and the data values are only given at these vertices. Without any loss in the generality of our state formulation (1), we assume that the points which constitute the state representation of the tracked instance I^n and all the finite element vertices have 1-to-1 correspondence, and each pair of corresponding points contain information for the same physical point. In other words, the data values at all the finite elements' vertices will contain the predicted complete motion state information at time *k*.

Having these arguments in hand for the suitability of this nonlinear model for our particular problem, we decided to incorporate the framework by Georgii and Westermann [GW08, GW05] for physical simulation of deformable volumetric bodies in real time, which is built upon the physical laws of continuum mechanics. Their framework is based on an implicit finite element method and it employs a multigrid approach for the efficient numerical simulation of elastic materials. Their proposed approach enabled us to do efficient realistic and numerically stable simulation of heterogeneous bodies (described by tetrahedral or hexahedral grids).

Regarding the set of boundary conditions at time *k*, denoted as $\mathbb{B}_k$, we check if the influence measure of the nearest-neighbor sample $s \in \mathbb{S}_k$ of every state point $\mathbf{P}_i$ is above some threshold, and only then compute $\mathcal{I}_k(\mathbf{P}_i)$ and add the pair $(\mathbf{P}_i, \mathcal{I}_k(\mathbf{P}_i))$ to the set $\mathbb{B}_k$. The influence measure is a function of the Euclidean distance between the nearest-neighbor sample $s \in \mathbb{S}_k$ and the respective state point $\mathbf{P}_i$. $\mathcal{I}_k$ is the identified best interpolant on $\mathbb{S}_k$, which currently employs a simple nearest-neighbor interpolation strategy.

An example of a finite element model of the CIRS triple modality (X-ray Mammography, MRI, Ultrasound) breast biopsy training phantom, is shown in Figure 5 right.

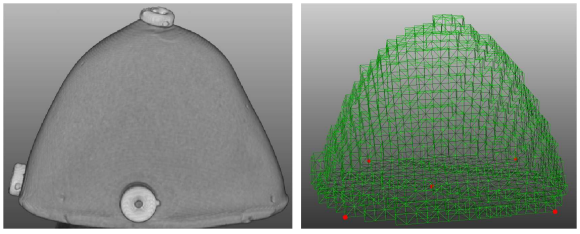

Figure 5: *Breast phantom. Left to right: MRI scan with 4 markers (one on the back side); the finite element-based model composed of tetrahedra elements which are extracted from the MRI scan data on the left. The points in red are fixated, i.e., the FEM-based nonlinear motion prediction model considers these vertices as not moving.*

The fixation points are chosen such that they reflect the expected realistic behavior of the motion which the breast phantom, shown in Figure 9, can undergo. The points $\mathbf{P}_i$, which constitute the state representation of the breast, have 1-to-1 correspondence with the tetrahedral finite element vertices, as depicted in Figure 6. Furthermore, the set of

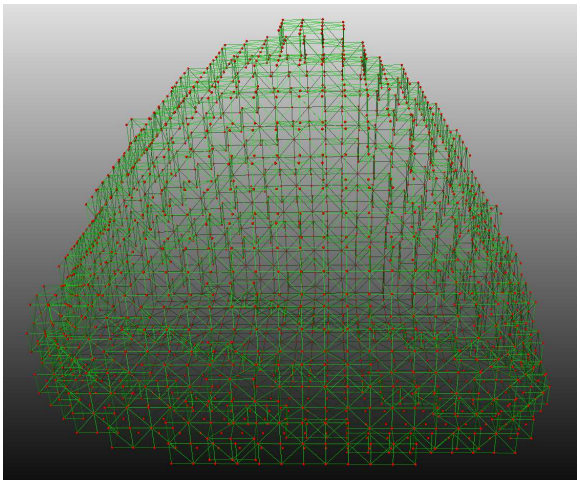

Figure 6: *1-to-1 correspondence between the points which constitute the state representation of the breast on one hand, and the tetrahedral finite element vertices on the other.*

boundary conditions $\mathbb{B}_k$ are applied on the tetrahedral finite element model on a per-vertex basis. We then compute the a priori displacement estimate $\mathcal{E}_k(\mathbf{P}_i)$ for all state points $\mathbf{P}_i$ for which a boundary condition is not provided, while taking into account the provided boundary conditions $\mathbb{B}_k$. In this regard, we employ a geometric multigrid solver on the tetrahedral grid to efficiently solve the resulting system of linear equations [GLDW10]. As the finite element-based model

is extracted from the MRI scan data, shown in Figure 5 left, and its material properties are set to match those of the CIRS phantom, the a priori displacement estimate $\mathcal{E}_k(\mathbf{P}_i)$ is actually the fusion of the motion dynamics and shape information sources at the state point $\mathbf{P}_i$. Furthermore, the a priori displacement estimate $\mathcal{E}_k(\mathbf{P}_i)$ serves as a prediction of the global motion signal at the state point $\mathbf{P}_i$, at time k.

6. A Posteriori State Estimation

While computing the a posteriori position estimate of each point $\mathbf{P}_i$, part of the state representation (1) of the tracked instance I^n (e.g., the breast phantom), we consider whether a boundary condition is provided for that state point or not. For all state points for which a boundary condition is provided in $\mathbb{B}_k$, we compute the a posteriori estimate as follows:

$$\widehat{\mathbf{P}}_\mathbf{i}(t_k) = \widehat{\mathbf{P}}_\mathbf{i}(t_{k-1}) + \mathcal{I}_k(\widehat{\mathbf{P}}_\mathbf{i}(t_{k-1})) \tag{4}$$

while for those for which it is not provided as:

$$\widehat{\mathbf{P}}_\mathbf{i}(t_k) = \widehat{\mathbf{P}}_\mathbf{i}(t_{k-1}) + \mathcal{E}_k(\widehat{\mathbf{P}}_\mathbf{i}(t_{k-1})) \tag{5}$$

where $\widehat{\mathbf{P}}_\mathbf{i}(t_{k-1})$ is the previous a posteriori position estimate of the state point $\mathbf{P}_i$. In other words, there are state points, on one hand, whose nearest-neighbor motion signal sampling point has a strong enough influence on them, while on the other hand there are state points whose nearest-neighbor motion signal sampling point does not have such a strong influence on them. Therefore the a posteriori position estimates of the former are computed using (4), while of the latter using (5).

7. Real-time Virtual Navigation Information Update

The virtual navigation information, e.g., a prior diagnostic MRI, shall be updated in real time according to the output of our intelligent information fusion engine, such that it reflects the estimated current shape and internal structure of the tracked breast instance. In our case, we decided to always display the MRI slice which corresponds to the current US 2D image. Therefore, the output of our information fusion engine at a discrete time k, i.e., the estimated state $\mathbf{S}(t_k)$, shall be used to update the prior MRI scan such that the corresponding MRI slice can be correctly sampled.

The prior MRI scan is taken at time t_0, i.e., when the motion state of the tracked breast is $\mathbf{S}(t_0)$. On the other hand, we have the displacement field which describes the motion of each state point $\mathbf{P}_i$ during the transition from state $\mathbf{S}(t_0)$ to state $\mathbf{S}(t_k)$. We could first move the MRI voxels, such that the 3D MRI scan reflects the estimated current shape of the tracked instance, and then sample the MRI volume at the plane corresponding to the US image plane. Alternatively, we could sample the above-described displacement field on the plane defined by the 2D US acquisition image, and then compute the MR image value for each plane pixel by sampling the MRI volume at the voxel which actually moved to the same plane point (based on the previously sampled displacement vector at the same pixel). We choose the latter approach for computing the corresponding MRI slice, because it avoids unnecessary computations. However, the sampling plane and the displacement field are both defined in the EM world coordinate system. Meaning, we also need to transform their descriptions to the MRI world coordinate system, in which the positions of the MRI voxel are described. Therefore, we need to compute the transformation between the EM and the MRI world coordinate systems.

The relationship between the EM and the MRI Cartesian coordinate systems, is found by using pair of measurements of the coordinates of four points in both systems. The measurements of the coordinates in the MRI world coordinate system are given by the 3D positions of the four MR markers (see Figure 5) in the MRI world, while their coordinates in the EM world coordiante system are acquired by pointing each of them with an EM-tracked sensor/pointer. The transformation parameters (rotation, translation, and scaling) are then found by employing the closed-form solution, by Umeyama [Ume91], of the general absolute orientation problem.

Figure 7 provides an example of a 2D US image together with its corresponding 2D MR slice, where the 2D MR slice is sampled, as described above, from the prior MRI scan of the breast phantom.

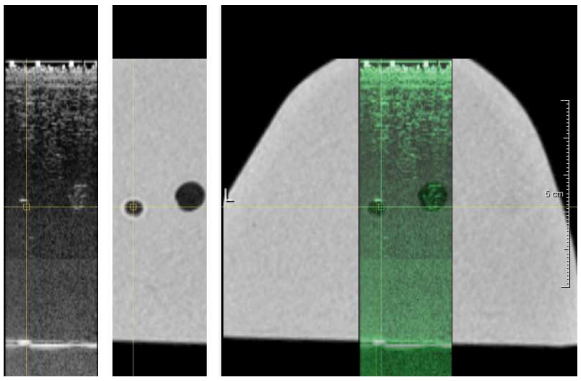

Figure 7: *US-MRI correspondence example. (Left to right) current US 2D image; corresponding MRI slice with the same extents as the current US 2D image; overlay of the current US 2D image on the full corresponding MRI slice.*

8. Concurrency and Parallelism Aspects

In order to make the estimation of the motion, a tracked instance I^n undergoes over time, possible in real time, we had to extensively parallelize each information source generation component as well as the overall information fusion engine. When striving for performance, programming in terms of threads (using low-level APIs) can be an inconvenient way to do multi-threaded programming. Logical tasks are a more

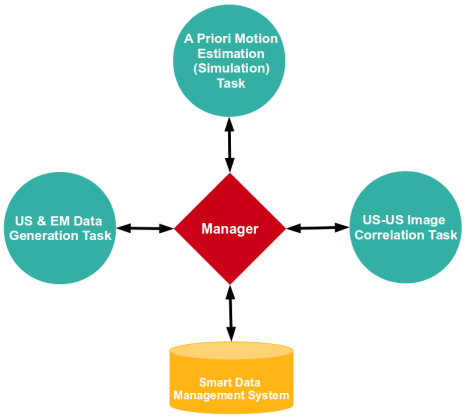

Figure 8: *Depiction of the communication flow in our intelligent information fusion system.*

appropriate choice, because they match better parallelism to available resources, have a faster start-up and shut-down, have a more efficient evaluation order, improved load balancing, and they provide higher-level thinking. Therefore, we have employed the Intel®Threading Building Blocks (Intel®TBB) library [Int], which supports scalable parallel programming using standard ISO C++ code. We define three different Intel®TBB-based logical tasks which can be described as follows:

1. a task which generates 2D ultrasound (US) images and electromagnetic tracking data in real time;
2. a task which performs the US-US image correlation in real time, and
3. a task which performs the fusion of the motion dynamics and the shape information sources (finite element-based simulation), i.e., the a priori motion estimation, in real time.

The communication and the synchronization between the different logical tasks is handled by a so called *Manager* unit (depicted in Figure 8), which we have implemented in addition. Furthermore, we had to devise a smart data management system to handle all data generated by the different tasks in a thread-safe manner.

The sampling of the displacement field (described in section 7) on the plane defined by the 2D US acquisition image, is extensively parallelized using OpenMP [OARB]. Furthermore, the 2D sampling of the prior MR image, based on the above-described sampled displacement field, is performed on the graphics processing unit (GPU).

9. Results and Discussion

The presented information fusion algorithm has been tested within our devised breast biopsy navigation system, depicted in Figure 9. This figure demonstrates the functionality of our information fusion engine, when estimating the global motion of the CIRS triple modality breast biopsy training phantom in real time.

The resolution of the input ultrasound (US) image, as shown in the top-left image viewer on the computer screen in Figure 9, is set to 512×512. Furthermore, the ultrasound acquisition depth is set to 120 mm.

The bottom-right image viewer, as depicted on the computer screen in Figure 9, shows an overlay of the two displacement vectors (capturing the local motion of the tracked breast lesions in the ultrasound image space) on the input US image. In this example, the global motion signal sampling data set $\mathbb{S}_k$ contains two samples from the output of the displacement function 2 on the breast interior spatial domain. Their sample values are set with the values of the overlaying displacement vectors, shown in the bottom-right image viewer on the computer screen in Figure 9, transformed to the EM world coordinate system. The set of boundary conditions $\mathbb{B}_k$, at time k, are then extracted from the set $\mathbb{S}_k$ and used as Dirichlet conditions [GLDW10] in the finite element model of the breast phantom.

The breast phantom is fixated with five pins. Two of them can be observed in front, while the remaining three cannot be seen because one is below (in the middle), and the other two behind the breast phantom (see Figure 9). One could also observe the virtual representation of these fixation points, rendered as red spheres, in the virtual scene containing the finite element model of the breast shown in the bottom-left image viewer on the computer screen in Figure 9, or more clearly in Figure 5.

For the performed tests, we used the following parameter configuration of the breast phantom finite element model:

Parameter	Value/Type
Integration Type	Dynamic Euler
Strain Type	Corotated Cauchy Strain
Stiffness	1000
Poisson Ratio	0.48
Density	1000
Damping	2.5
Time Step	0.033
Number of VCycles	1

Having set the finite element model with the above information, we are able to compute the a priori displacement estimate $\mathcal{E}_k(\mathbf{P}_i)$ for all state points $\mathbf{P}_i$ for which a boundary condition is not given.

Then, we are able to compute the a posteriori position estimate for all state points $\mathbf{P}_i$, as described in Section 6.

Furthermore, we are able to continuously update the prior diagnostic image (in this example an MRI image), based on the real-time output of our fusion algorithm, as described in 7. In the top-right image viewer on the computer screen in Figure 9, one could observe that the updated diagnostic MRI image map reflects the true shape and internal structure of the examined breast (see also Figure 7). In this way, we

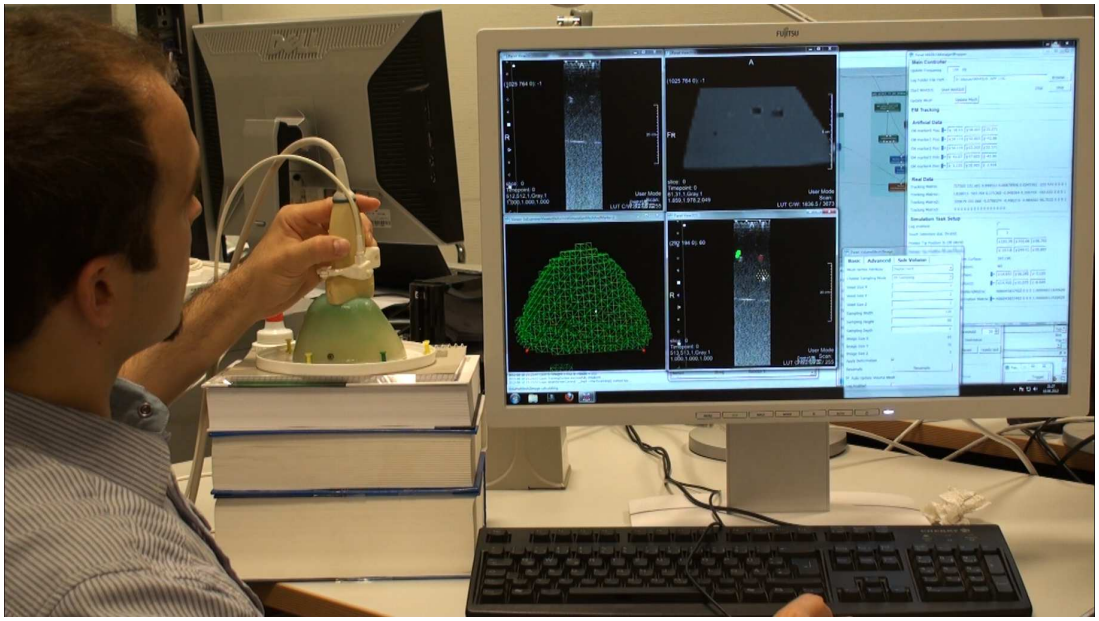

Figure 9: *Hybrid Image-guided Breast Biopsy Navigator. (Please see the accompanying video material.)*

can actually claim that we are also able to provide a hybrid image-guided (in this example US-MRI-guided) biopsy navigation.

We analyzed the real-time performance of our information fusion system on a desktop PC (Intel(R) Core(TM) 2 Quad CPU Q9000 @ 2.00 GHz 2.00 GHz, 4 GB RAM, Windows 7 Professional 64 bit) and obtained that on average we achieve 20-30 updates of the current state per second. The non-constant update rate is mainly due to the concurrent nature of the different components in the information fusion engine.

However, the accuracy of our information fusion system has only been visually inspected in our laboratory setting using the CIRS phantom and not yet for estimating the motion of deformable human organs in an intervention room. In future work, we plan on first validating the results of our information fusion algorithm against simulated ground-truth global motion signal values. One could simulate the ground-truth global motion signal using the finite element model of the soft-tissue tracked instance. Then one would need to sample the ground-truth global motion signal at locations which do not necessarily correspond to the state points $\mathbf{P}_i$, and use these samples as ground-truth global motion signal samples. These samples would constitute the motion measurements information source which will be fused with the dynamics and the shape information sources by our fusion engine. The result will be then compared against the above-specified ground-truth global motion signal. For an overall system validation, we plan on generating the ground-truth navigation information for a certain number of time points (e.g., by acquiring MRI scans of the deformed soft-tissue tracked instance at the respective time points) and comparing it against the updated virtual navigation information (e.g., the deformed prior MRI scans) based on the output of our information fusion algorithm at the respective time points.

10. Conclusion and Future Work

We devised an intelligent information fusion engine for real-time estimation of the motion that a tracked instance undergoes over time. The engine fuses the tracked instance's motion dynamics, motion measurements, and shape information sources. As a result, all available knowledge in the information space is combined.

We incorporated electromagnetic bodies/sensors for sampling the global motion signal on the deformable organ's surface spatial domain. For sampling the global motion signal on the deformable organ's interior spatial domain, we used an appropriate real-time US-US image correlation algorithm which identifies distinctive soft-tissue structures and tracks them over time.

By employing a finite element model, we were able to best model, based on the theory of elasticity, the dynamics of the motion which a deformable organ undergoes over time. Using this nonlinear motion model, we were able to predict, in real time, the change in the motion deformation component from time $k-1$ to k.

We showcased the feasibility of our devised information fusion engine by employing it for capturing the global motion of a breast phantom during an image-guided biopsy. In this way, we enabled the real-time update of the biopsy planning

navigation data according to the posteriori estimate of the global motion. In return, the real-time changes in the shape of the breast are always reflected in the navigation information.

As we assumed error-free measurements and modeling, our a posteriori position estimates depend either only on the interpolated displacement or only on the a priori displacement estimate. In other words, currently we do not model the uncertainties neither in the electromagnetic tracking nor in the US-US image correlation data. In future work, we plan on quantifying these uncertainties and including this knowledge in the information space. This will enable us to incorporate the uncertainty information source in the a posteriori state estimation, such that a proper (always assuring consistent and conservative a posteriori position estimates) uncertainty-aware information fusion is possible.

Acknowledgements

This work was supported by the Fraunhofer Internal Programs under Grant No. MAVO 823 287.

References

[AM79] ANDERSON B. D., MOORE J. B.: *Optimal Filtering*. Prentice-Hall, 1979. 3

[BFMR08] BAUMHAUER M., FEUERSTEIN M., MEINZER H.-P., RASSWEILER J.: Navigation in endoscopic soft tissue surgery: perspectives and limitations. *Journal of endourology 22*, 4 (2008), 751–766. 3

[CMS*05] CASH D. M., MIGA M. I., SINHA T. K., GALLOWAY R. L., CHAPMAN W. C.: Compensating for intraoperative soft-tissue deformations using incomplete surface data and finite elements. *Medical Imaging, IEEE Transactions on 24*, 11 (2005), 1479–1491. 3

[CZK04] COMANICIU D., ZHOU X. S., KRISHNAN S.: Robust real-time myocardial border tracking for echocardiography: an information fusion approach. *Medical Imaging, IEEE Transactions on 23*, 7 (2004), 849–860. 2, 4

[DTC*10] DUMPURI P., THOMPSON R. C., CAO A., DING S., GARG I., DAWANT B. M., MIGA M. I.: A fast and efficient method to compensate for brain shift for tumor resection therapies measured between preoperative and postoperative tomograms. *Biomedical Engineering, IEEE Transactions on 57*, 6 (2010), 1285–1296. 3

[DTD*07] DUMPURI P., THOMPSON R. C., DAWANT B. M., CAO A., MIGA M. I.: An atlas-based method to compensate for brain shift: Preliminary results. *Medical Image Analysis 11*, 2 (2007), 128–145. 3

[GD12] GEORGII J., DICK C.: Efficient finite element methods for deformable bodies in medical applications. *Critical Reviews^{TM} in Biomedical Engineering 40*, 2 (2012), 155–172. 6

[GLDW10] GEORGII J., LAGLER D., DICK C., WESTERMANN R.: Interactive deformations with multigrid skeletal constraints. In *Proceedings of the 7th Workshop On Virtual Reality Interaction and Physical Simulation* (2010), pp. 39–47. 6, 8

[GW05] GEORGII J., WESTERMANN R.: A multigrid framework for real-time simulation of deformable volumes. In *Workshop On Virtual Reality Interaction and Physical Simulation* (2005). 6

[GW08] GEORGII J., WESTERMANN R.: Corotated finite elements made fast and stable. In *Proceedings of the 5th Workshop On Virtual Reality Interaction and Physical Simulation* (2008), pp. 11–19. 6

[Hor87] HORN B. K.: Closed-form solution of absolute orientation using unit quaternions. *JOSA A 4*, 4 (1987), 629–642. 3

[IB98] ISARD M., BLAKE A.: Condensation-conditional density propagation for visual tracking. *International journal of computer vision 29*, 1 (1998), 5–28. 5

[Int] INTEL: Intel Threading Building Blocks. https://www.threadingbuildingblocks.org. 8

[KOP11] KOCEV B., OJDANIC D., PEITGEN H.: An approach for projector-based surgeon-computer interaction using tracked instruments. In: Proc. of GI Workshop: Emerging Technologies for Medical Diagnosis and Therapy. 2

[KRL13] KOCEV B., RITTER F., LINSEN L.: Projector-based surgeon-computer interaction on deformable surfaces. *International Journal of Computer Assisted Radiology and Surgery* (2013), 1–12. URL: http://dx.doi.org/10.1007/s11548-013-0928-1, doi:10.1007/s11548-013-0928-1. 2, 3

[MHJW12] MILLER K., HORTON A., JOLDES G., WITTEK A.: Beyond finite elements: A comprehensive, patient-specific neurosurgical simulation utilizing a meshless method. *Journal of biomechanics 45*, 15 (2012), 2698–2701. 3

[MMHW*08] MEINZER H.-P., MAIER-HEIN L., WEGNER I., BAUMHAUER M., WOLF I.: Computer-assisted soft tissue interventions. In *Biomedical Imaging: From Nano to Macro, 2008. ISBI 2008. 5th IEEE International Symposium on* (2008), IEEE, pp. 1391–1394. 1

[NMK*05] NEALEN A., MÜLLER M., KEISER R., BOXERMAN E., CARLSON M.: Physically based deformable models in computer graphics. In *Proceedings of Eurographics* (2005), pp. 71–94. 3

[OARB] OPENMP ARCHITECTURE REVIEW BOARD: OpenMP. http://openmp.org. 8

[RNN10] RAJAGOPAL V., NIELSEN P. M., NASH M. P.: Modeling breast biomechanics for multi-modal image analysisâĂŤsuccesses and challenges. *Wiley Interdisciplinary Reviews: Systems Biology and Medicine 2*, 3 (2010), 293–304. 3

[ŠND02] ŠKRINJAR O., NABAVI A., DUNCAN J.: Model-driven brain shift compensation. *Medical Image Analysis 6*, 4 (2002), 361–373. 3

[Ume91] UMEYAMA S.: Least-squares estimation of transformation parameters between two point patterns. *IEEE Transactions on pattern analysis and machine intelligence 13*, 4 (1991), 376–380. 7

[ZBL*06] ZHANG H., BANOVAC F., LIN R., GLOSSOP N., WOOD B. J., LINDISCH D., LEVY E., CLEARY K.: Electromagnetic tracking for abdominal interventions in computer aided surgery. *Computer Aided Surgery 11*, 3 (2006), 127–136. 3

[ZGB10] ZHANG X., GÜNTHER M., BONGERS A.: Real-time organ tracking in ultrasound imaging using active contours and conditional density propagation. In *Medical Imaging and Augmented Reality*. Springer, 2010, pp. 286–294. 5

[ZGC05] ZHOU X. S., GUPTA A., COMANICIU D.: An information fusion framework for robust shape tracking. *Pattern Analysis and Machine Intelligence, IEEE Transactions on 27*, 1 (2005), 115–129. 4